ARTICLE

Super-Robust, Lightweight, Conducting Carbon Nanotube Blocks Cross-Linked by De-fluorination

Yoshinori Sato,[†,*] Makoto Ootsubo,[†] Go Yamamoto,[‡,§] Gregory Van Lier,[⊥,*] Mauricio Terrones,[∥,*] Shinji Hashiguchi,[#] Hisamichi Kimura,[¶] Akira Okubo,[¶] Kenichi Motomiya,[†] Balachandran Jeyadevan,[†] Toshiyuki Hashida,[§] and Kazuyuki Tohji[†]

[†]Graduate School of Environmental Studies, Tohoku University, Aoba 6-6-20, Aramaki, Aoba-ku, Sendai 980-8579, Japan, [‡]Institute of Fluid Science, Tohoku University, 2-2-1, Katahira, Aoba-ku, Sendai 980-8577, Japan, [§]Fracture and Reliability Research Institute, Graduate School of Engineering, Tohoku University, Aoba 6-6-11, Aramaki, Aoba-ku, Sendai 980-8579, Japan, [⊥]Research Group General Chemistry, Free University of Brussels, Pleinlaan 2, B-1050 Brussels, Belgium, [∥]Advanced Materials Department, IPICyT, Camino a la Presa San José 2055, Lomas 4a seccion 78216, San Luis Potosí, SLP, México, [#]Stella Chemifa Corporation, 1-41, Rinkai-cho, Izumiotsu, Osaka 595-0075, Japan, and [¶]Institute for Materials Research, Tohoku University, 2-2-1, Katahira, Aoba-ku, Sendai 980-8577, Japan

ABSTRACT We produced large binder-free multi-walled carbon nanotube (MWNT) blocks from fluorinated MWNTs using thermal heating and a compressing method *in vacuo*. This technique resulted in the formation of covalent MWNT networks generated by the introduction of sp^3-hybridized carbon atoms that cross-link between nanotubes upon de-fluorination. The resulting carbon nanotube blocks are lighter than graphite, can be machined and polished, and possess average bending strengths of 102.2 MPa, a bending modulus of 15.4 GPa, and an electrical conductivity of 2.1×10^2 S/cm. Although each nanotube exhibits a random structure in these blocks, the mechanical properties are 3 times higher than those obtained for commercial graphite. On the basis of theoretical molecular dynamics simulations, a model is presented for the nanotube interconnecting mechanism upon de-fluorination.

KEYWORDS: carbon nanotubes · blocks · fluorine · binder-free · strength · conducting · solidification

Robust blocks containing pure carbon nanotubes (CNTs) in the absence of a binder are expected to be applicable in (a) the fabrication of electrodes and biomaterials for supercapacitors,[1] bioelectrodes, and biosensors,[2] (b) cell growth scaffolding,[3] (c) dental implants, and (d) artificial bone structures.[4] These materials could take advantage of the outstanding characteristics of individual CNTs, which possess a high surface area and fascinating electronic and mechanical properties.[5] In addition, the synthesis of covalent two-dimensional (2D) and three-dimensional (3D) carbon-network nanomaterials from one-dimensional (1D) building blocks (CNTs) is gaining importance due to their fascinating mechanical and electronic properties that have been predicted recently.[6] However, it has proved difficult to solidify pure CNTs in the absence of a binder. Narrow-diameter (<1–2 nm) single-walled carbon nanotubes (SWNTs) that are highly curved could be more chemically active (when compared to planar graphite)[7–11] due to a rehybridization effect[12] and the strain energy.[13] Since the strain energy is inversely related to the nanotube diameter, a large-diameter nanotube (>2 nm) is thermodynamically and chemically stable. Therefore, large-diameter CNTs (similar to graphite sheets) are normally inert, and reactions on their surfaces are difficult if no structural defects are present. In this context, numerous scientists have faced various difficulties in incorporating large-diameter CNTs (multi-walled) into polymeric, metallic, or ceramic matrices due to their weak adhesion (interaction) that does not permit the formation of sp^3-hybridized carbon atoms between the tube walls and the matrix.[14] Thus, pure CNT composite assemblies have the disadvantage that the load is not efficiently transferred to the tubes due to the weak adhesion. This results in tubes slipping within the matrix, and the formation of sp^3-hybridized carbon atoms that are established among nanotubes is significantly inhibited.[15] However, some studies have reported the local coalescence[16,17] and cross-linking polymerization[18,19] of SWNTs and double-walled carbon nanotubes using high electron irradiation in conjunction with thermal heating, resulting in the generation of vacancies on the nanotubes that aid in the establishment of sp^3-like carbon atoms. It is therefore important to develop a method for producing efficient cross-linking sites (*via* the formation of defects or vacancies)

*Address correspondence to hige@bucky1.kankyo.tohoku.ac.jp (Y.S.), gvanlier@nanoscience.be (G.V.L.), mterrones@titan.ipicyt.edu.mx (M.T.).

Received for review October 26, 2007 and accepted January 15, 2008.

Published online February 8, 2008. 10.1021/nn700324z CCC: $40.75

on bulk nanotubes' surfaces so that the generation of sp^3-hybridized carbon atoms and tube interconnections is increased between individual nanotubes.

In this study, we demonstrate that an advantageous method for producing active cross-linking sites on the surface of nanotubes could proceed *via* defluorination of multi-walled carbon nanotubes (MWNTs). Fluorination of CNTs is a very important functionalization method, since it can reach C_2F stoichiometries corresponding to the tube surface coverage. In addition, fluorination could improve solubility and processability, and could also be followed by full defunctionalization.[20,21] In particular, de-fluorination of fluorinated SWNTs is carried out *via* thermal treatments at 673–1237 K *in vacuo*; volatile fluorinated carbonaceous molecules such as CF_x are formed,[21,22] and defluorinated SWNTs could then exhibit active sites all over their surface. Here we report on the production of free-standing solidified MWNT blocks by defluorinating fluorinated MWNTs. We found that these blocks reveal excellent mechanical and electronic properties. We compared the properties of these blocks with those of block samples of carboxylated MWNTs upon defunctionalization (de-COOH-MWNT blocks) and commercial graphite (IG-11; fine-graphited isotropic graphite, Toyo Tanso Co., Ltd.; see Materials and Methods). We found that the method described here is able to introduce a large number of sp^3-hybridized carbon atoms that cross-link the nanotubes when the spark plasma sintering (SPS) system operates at pressures under 80 MPa and 1273 K for 10 min (see Materials and Methods and Supporting Information, Figure S1). We further propose a cross-linking mechanism based on molecular dynamics (MD) simulations of de-fluorinated nanotubes.

RESULTS AND DISCUSSION

In this study, we used MWNTs (NanoLab, Inc. USA) synthesized by chemical vapor deposition (CVD). These MWNTs exhibited a bamboo-like multilayered structure (Figure 1). The procedure for the purification of MWNTs and the fluorination procedure are described in the Materials and Methods. The size and shape of defluorinated MWNT (de-F-MWNT) blocks depend on the size and shape of the graphite die and the quantity of the fluorinated MWNTs used (Figure 2a). It is noteworthy that the produced blocks of MWNTs do not break and can be processed further (cutting and polishing; note that purified pristine MWNTs cannot be manufactured). Figure 2b,c depicts the typical low- and high-magnification scanning electron microscopy (SEM) images of the fracture surface of a de-F-MWNT block (the inset in Figure 2b corresponds to the SEM image of the fractured piece). In these blocks, MWNTs were found embedded in the whole cross section (Figure 2c). As can be seen on the fracture surface, each individual MWNT was observed and seemed to have excellent contact

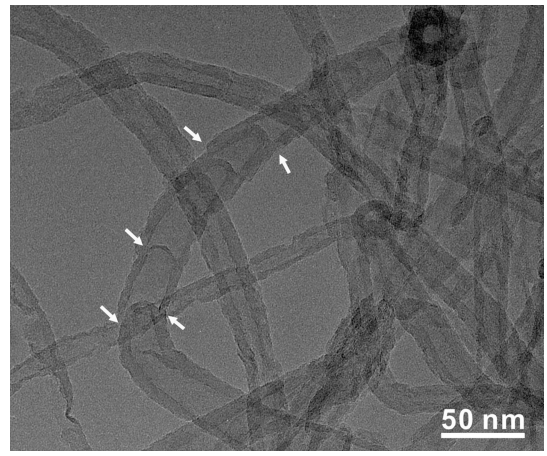

Figure 1. TEM image of typical of bamboo-like MWNTs depicting compartmentalized structures (see arrows).

along the nanotube axis. Other carbon materials were notably absent under the present conditions. It has been reported that MWNTs and SWNTs could be transformed into diamond-like carbon and graphite under high pressures and high temperatures.[18,23–25] The processing temperature, pressure, and graphitization of carbon nanotubes used in this study were crucial to efficiently bind the tubes. High-resolution transmission electron microscopy (HRTEM) observations of fragmented blocks containing de-F-MWNTs showed MWNTs to be in contact with or cross-linked to neighboring nanotubes (see arrows in Figure 2d,e). In addition, highly compacted agglomerates of de-F-MWNTs were also observed (Figure 2f). The HRTEM images of fluorinated MWNTs indicate an increase in the interlayer spacing only between the outer shells following their fluorination, while the inner layers remained crystalline. The distances between dark fringes (002 interlayer spacing) measured by HRTEM were estimated to be 0.58 ± 0.03 nm on average (see arrows in Figure 3a), whereas the (002) interlayer spacing of de-F-MWNT blocks was found to be approximately 0.34 nm (Figure 3b).[26,27] From the X-ray powder diffraction (XRD) pattern, we observed a new peak appearing at *ca.* $2\theta = 13.3°$, which is attributed to the (001) reflection of fluorinated graphite (see Supporting Information, Figure S2). The (001) interlayer spacing of fluorinated MWNTs was found to be 0.67 ± 0.07 nm, and these intensities disappeared in the de-F-MWNT blocks. Both HRTEM and XRD studies indicate that fluorination and defluorination were successful. The de-fluorinated MWNTs also exhibit a good crystallinity within the layers, as revealed by the presence of a sharp reflection of the graphite (002) plane (see Supporting Information). Based on previous thermal studies of fluorinated SWNTs,[22,27–29] part of the fluorinated carbon molecules were driven off the sidewall or the outside interlayer of fluorinated MWNTs as CF_2, CF_3, and CO_2 upon heating partially fluorinated MWNTs (*e.g.*, from 763 to 823 K in an Ar atmosphere). These data indicate that the

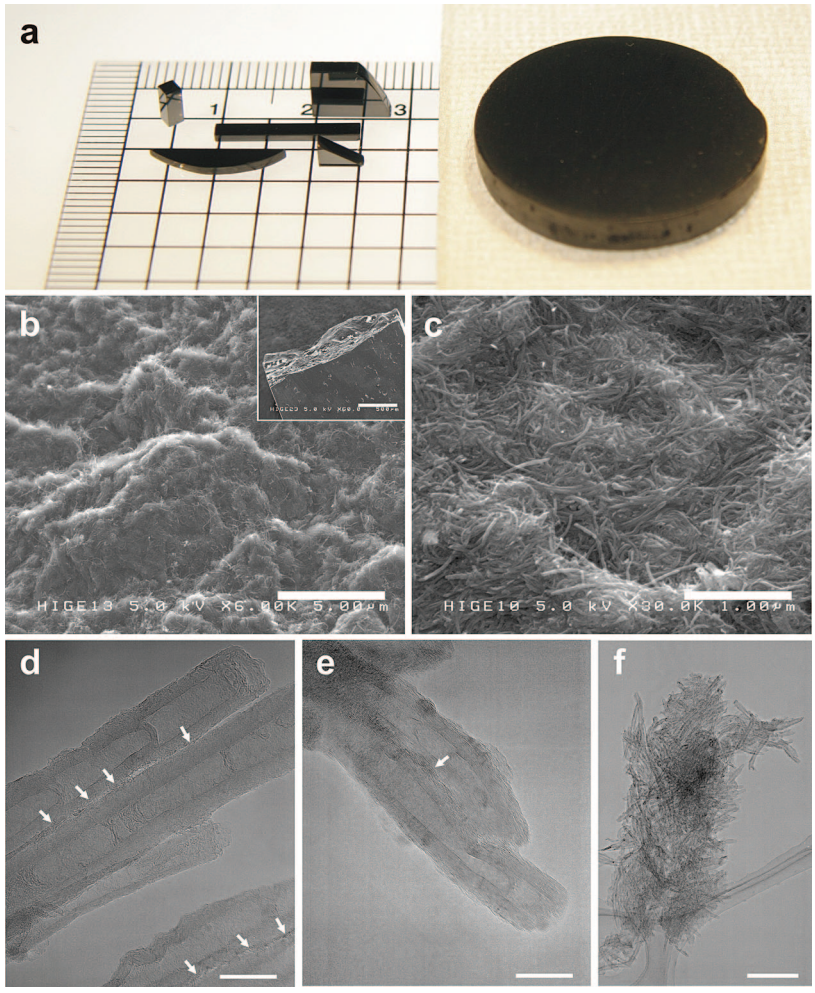

Figure 2. De-F-MWNT blocks. (a) Picture of various shapes of de-F-MWNT blocks. (b) Low-magnification SEM image of the fracture surface of a typical de-F-MWNT block (scale bar, 5.0 μm). The inset depicts the SEM image of the fractured piece of the specimen (scale bar, 500 μm). (c) High-magnification SEM image of the fracture surface of the de-F-MWNT blocks (scale bar, 1.0 μm). (d,e) High-magnification HRTEM images of the fragmented de-F-MWNT blocks. Arrows indicate parts in which the MWNTs seem to be in contact or cross-linked parallel to each other (scale bar, 25 nm). (f) Low-magnification HRTEM image of agglomerated nanotubes within de-F-MWNT blocks (scale bar, 300 nm).

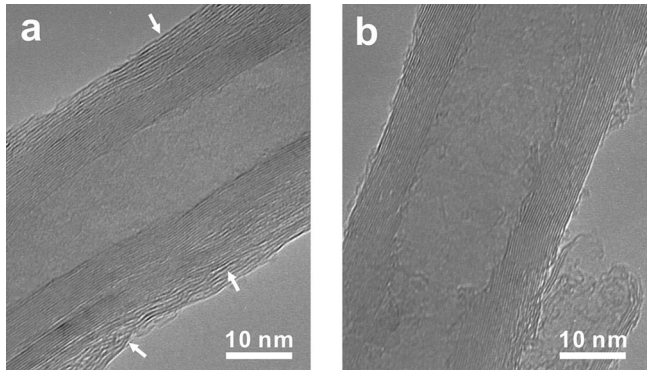

Figure 3. HRTEM images of fluorinated and de-fluorinated MWNTs. (a) HRTEM image of fluorinated MWNTs. The outside layers show the fluorinated layers with average interlayer spacings of 0.58 ± 0.3 nm (see arrows). (b) HRTEM image of the MWNTs found in the de-F-MWNT blocks. The interlayer spacing of MWNT is *ca.* 0.34 nm (similar to that found in purified MWNTs).

thermolysis of fluorinated MWNTs results in the formation of volatile carbon−fluorine-containing molecules and not simply by the loss of fluorine gas. In order to explain the SPS solidification, we believe that, as the carbon−fluorine gases are liberated, vacancies and other defects on the surface of MWNTs are generated and make the tubes more reactive. The formation of CO_2 is due to the presence of oxygen atoms in different functional groups attached to the nanotube surface, typically originating from the purification procedure (*e.g.*, −COOH or −OH).

As shown in the X-ray photoelectron spectroscopy (XPS) spectrum (see Figure 4a), our fluorinated MWNTs exhibited two main peaks at 284.5 and 288.0 eV, which correspond to a carbon bonded to a bare carbon atom, and a single F atom, respectively.[29] We found CF_x ($x = 0.40-0.52$) stoichiometries by integrating the intensities of these two C_{1s} peaks.[30] After the SPS process of fluorinated MWNTs, the XPS spectrum reveals only one peak located at 284.3 eV, which indicates that carbon−fluorine bonding disappears; this confirms de-fluorination of the MWNTs. It is also important to note that, in the FT-IR spectra of carbon nanotubes with a higher defect concentration, a broader band located at 1200 cm^{-1} is usually observed.[31−34] In our case, we confirmed that, following fluorination, an intense band at 1211 cm^{-1} appeared, characteristic of the C−F covalent bond (Figure 4b).[26] Interestingly, the band of the C−F covalent bond disappeared from the FT-IR spectrum of de-F-MWNT blocks, and a broader band located at 1203 cm^{-1} remained from the carbon skeleton, which could be related to the bonding information of sp^3-hybridized orbitals at the contact points of numerous MWNTs.

In Figure 4c, Raman spectra of different MWNTs are depicted, and a pair of peaks is observed around 1340 cm^{-1} (D-band) and 1580 cm^{-1} (G-band). The intensity ratio, I_D/I_G, is known to depend on the number of defects within the nanotubes (disorder-induced band). As shown in Figure 4c, the I_D/I_G ratio of fluorinated MWNTs is 1.18, thus confirming the presence of C−F sp^3-hybridized carbon atoms. On the other hand, the defect ratio for the de-F-MWNT ($I_D/I_G = 1.20$) is larger when compared to that of purified MWNTs ($I_D/I_G = 0.90$). This indicates that the presence of defective carbon networks with sp^3 hybrid orbitals increased after de-fluorination of nanotubes. In addition, the D-band could also be related to the presence of sp^3-hybridized carbon atoms located at the contact points of neighboring MWNTs.[18,35]

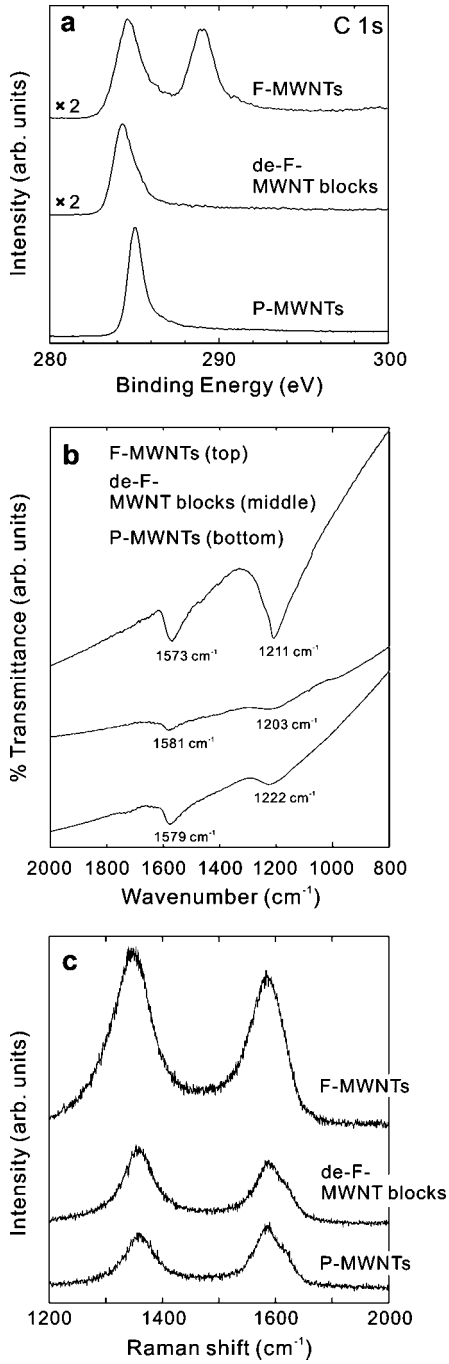

Figure 4. XPS, FT-IR, and Raman spectra of de-F-MWNT blocks. (a) XPS C_{1s} spectra of fluorinated MWNTs (top), de-F-MWNT blocks (middle), and purified MWNTs (bottom). (b) FT-IR spectra of fluorinated MWNTs (top), de-F-MWNT blocks (middle), and purified MWNTs (bottom). (c) Raman spectra of tangential modes for fluorinated MWNTs (top), de-F-MWNT blocks (middle), and purified MWNTs (bottom). The wavelength of the laser line was 488.0 nm.

Table 1 shows the physical, electrical, and mechanical properties of de-F-MWNT blocks. In order to highlight the effects of fluorine, we also performed experiments with functionalized nanotubes containing COOH or OH functional groups. In this case, de-COOH-MWNT blocks were produced under conditions similar to those used for de-fluorinated MWNTs (see Materials and Methods section). For example, the densities of de-F-MWNT blocks (1.44 g/cm^3) and de-COOH-MWNT blocks (1.34 g/cm^3) are by far lighter than that of commercial graphite (1.74 g/cm^3). The porosity of de-F-MWNT blocks (36.2%) is slightly smaller than that of de-COOH-MWNT blocks (40.7%). This indicates that the number of contact (binding) points among the nanotubes increased, and the densification of de-F-MWNT blocks was enhanced. We believe that the porosity is caused by defects created by defluorination and intertube free spaces found in the blocks.

TABLE 1. Physical, Electrical, and Mechanical Properties for the de-F-MWNT Blocks, the de-COOH-MWNT Blocks, and Commercial Graphite (Reference Sample)

characteristic	de-F-MWNT blocks	de-COOH-MWNT blocks	commercial graphite (IG-11)
bulk density, ρ (g/cm^3)	1.44	1.34	1.74
porosity (%)	36.2	40.7	23.0
Young's modulus, E_b (GPa)	14.2–16.3	6.4–7.8	6.5–8.6
fracture bending strength, σ_b (MPa)	92.4–123.0	29.0–47.6	42.1–43.7
Vickers hardness, H_v(MPa)	46.9	33.2	16.8
conductivity, σ (S/cm) (four-probe method)	2.1×10^2	1.5×10^2	6.0×10^2

The fracture bending strength and Young's modulus (bending modulus) of de-F-MWNT blocks were on average 102.2 MPa (min 92.4 MPa, max 122.7 MPa) and 15.4 GPa, respectively (Figure 5a). These values are 3 times and 2 times larger than those observed for de-COOH-MWNT blocks (fractural bending strength of 38.2 MPa, Young's modulus of 7.3 GPa) or commercial graphite (fractural bending strength of 43.7 MPa, Young's modulus of 7.6 GPa), respectively. On the fracture surface, nanotubes with both opened and closed tips were observed (Figure 5b,c). It seems likely that, due to the bamboo-like structure of nanotubes, the fragments (swords) were separated from the main body of the body (sheath; see Figure 5d).[36] In order to understand how MWNTs behave upon bending within the solid blocks, we first noted that the nanotubes do not pull out but rather break when the CNT blocks are fractured (see Figure 5b−d). In particular, we observed that the outside layers of the MWNTs were destroyed by the tensile stress during the bending test. Subsequently, the bamboo-like MWNTs (sword) could easily be pulled out due to the small static or dynamic friction force between the concentric layers (see Figure 5d).[37] Thus, it is of great importance that the nanotube structure (*e.g.*, concentric and perfect cylinders or bamboo-type morphologies) and the degree of crystallinity within the tubes, as

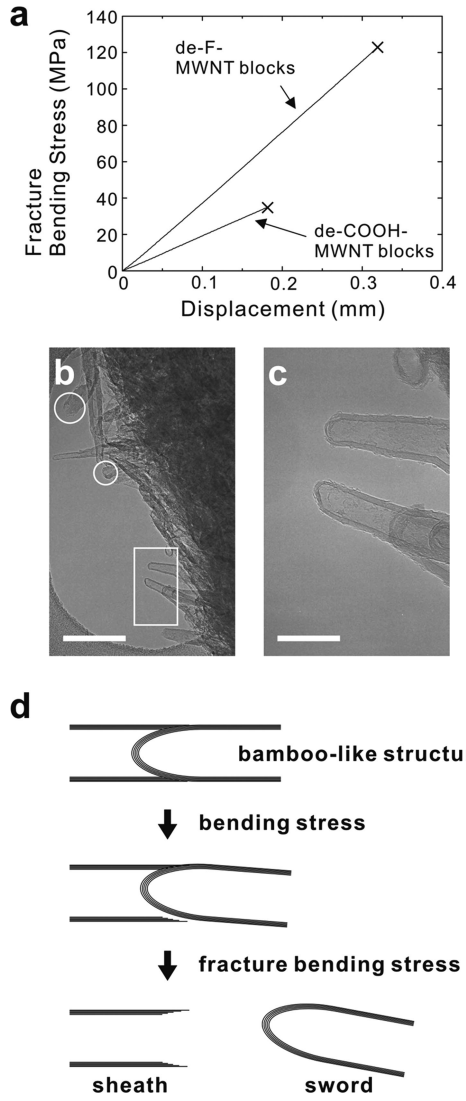

Figure 5. Fracture bending stress of de-F-MWNT blocks. (a) Typical stress *vs* load-line displacement curve comparing de-F-MWNT blocks and de-COOH-MWNT blocks. (b) Low-magnification HRTEM image of the fracture surface of the de-F-MWNT blocks (scale bar, 100 nm). Typical MWNTs marked in white circles and the square show the opened and closed tips, respectively. (c) High-magnification HRTEM image of the area in the white square shown in panel b (scale bar, 25 nm). (d) Schematic illustration of the breaking mechanism of the bamboo-like section of a MWNT. When the bending stress is applied to the bamboo-like compartment, the core with a closed tip (sword) is separated from the body (sheath).

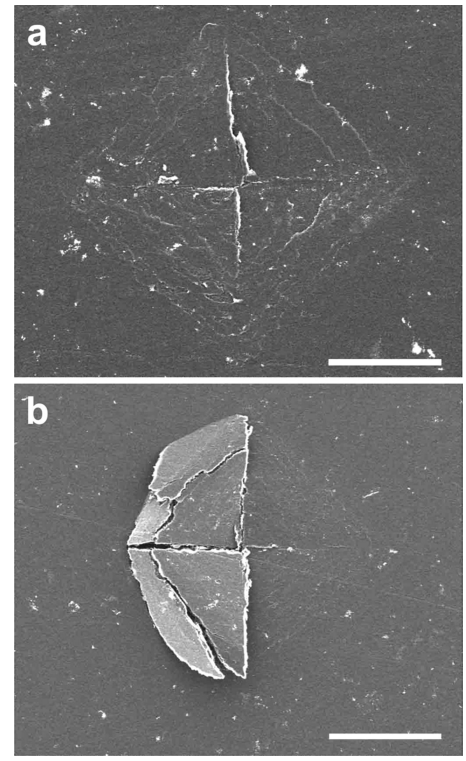

Figure 6. Hardness of de-F-MWNT blocks. (a) Typical SEM top-view image of a Vickers indentation site for de-F-MWNT blocks (scale bar, 30 μm). There is no evidence of classical radial cracks. (b) SEM top-view image of a Vickers indentation site for de-F-MWNT blocks (scale bar, 37.5 μm). Elastic recovery was observed after the load was removed.

well as the presence of defects or vacancies on their surface, are carefully controlled since they could significantly alter the mechanical strength of the nanotubes, and hence the mechanical properties of the bulk nanotube blocks.

It is also noteworthy that, on the fracture surface of de-COOH-MWNT blocks, nanotubes are less compacted (not firmly bound to the block) and appear with closed and open tips (see Supporting Information, Figure S3). In this particular case, it seems like each nanotube slipped (pulled out) from the block, since the nanotubes are not firmly joined together. However, for de-F-MWNT blocks, it appears that nanotube pull-outs are prevented, due to the increased presence of nanotube cross-links. The Vickers indentation test measures the hardness of materials. Figure 6a shows representative SEM images of a Vickers indentation site for de-F-MWNT blocks; note the absence of classical cracks. The Vickers hardness is on average 46.9 MPa, and for some indentation sites, elastic recovery was observed after removing the load (Figure 6b). These Vickers indentation results clearly indicate that de-F-MWNT blocks are highly resistant to contact damage and confirm the elastic flexibility of carbon nanotubes.[38]

We also measured the macroscopic electrical conductivity on some of the de-F-MWNT blocks at room temperature using a four-probe method. The average electrical conductivity of de-F-MWNT blocks was 2.1×10^2 S/cm. The conductivity of the fluorinated MWNTs (powder) was 4.7×10^{-6} S/cm when using a pressure-induced electrical resistivity method (bulk density, 1.44 g/cm^3). It has been demonstrated that fluorinated graphite and fluorinated SWNTs exhibit low electrical conductivity values, but this value could change significantly after de-fluorination.[39] Our electrical transport results confirm that de-fluorination indeed took place. The electrical conductivity ratio between the horizontal and thickness direction of the de-F-MWNT, mea-

sured by the two-probe method, shows a large anisotropy of about 15–30. This originates from the MWNTs being solidified in the horizontal direction, as shown in Figure 2c.

Terrones *et al.* reported that the creation of vacancies induce coalescence of nanotubes *via* a zipper-like mechanism, imposing a continuous reorganization of atoms on individual tube lattices along adjacent tubes.[16] The presence of vacancies and related defects (*e.g.*, divacancies) results in deformation of C−C nanotube bonds so as to form coalesced or polymerized carbon nanotubes. In order to model the de-fluorination process and the subsequent cross-linking between adjacent nanotubes, theoretical MD simulations were performed using the atom-centred density matrix propagation (ADMP) molecular dynamics model[40–42] at the AM1 semiempirical level of theory using Gaussian03.[43] As a model system, we calculated two independent and adjacent (5,5) open SWNTs of 240 carbon atoms each, which were hydrogen terminated ($C_{240}H_{20}$). We also considered a tube interspacing equal to twice their van der Waals radius. The same system was also considered with fluorination along the tube axis (C_2F addition pattern).[44] The fluorinated systems resulted in two adjacent $C_{240}F_{100}H_{20}$ carbon nanotubes. All calculations were performed at 4000 ± 20°C. Under these conditions, the carbon nanotubes remain unconnected and the hexagonal lattice is retained, both when two adjacent pristine nanotubes are considered and for two adjacent fluorinated carbon nanotubes. In addition, when point defects were introduced in the hexagonal lattice of the pristine nanotubes (two vacancies created on each nanotube at their interface), no cross-linking occurred between the nanotubes. However, when the same calculations were run for two adjacent fluorinated nanotubes with the same point defects (see Figure 7a), the nanotube structure started to deteriorate significantly over time, and dangling bonds started to appear around the defect sites (see Figure 7b,c). NT—C≡C—F and NT═CF_2 functional groups were observed during these simulations. From our results, it can be concluded that, upon de-fluorination, the defect sites present on the nanotube surface are responsible for the formation of CF_x species and act as starting points for establishing the cross-linking of the outer graphene layers. In other words, the hexagonal lattice is expected to break up at these defective sites, thus creating dangling bonds. On these sites, bonding between adjacent nanotubes is very likely upon further de-fluorination. We note that, although perfect covalent bonding between nanotubes was not observed during the MD simulations, these do not consider any external pressure, as opposed to the experimental setup. Therefore, external pressure is expected to approach the nanotubes dur-

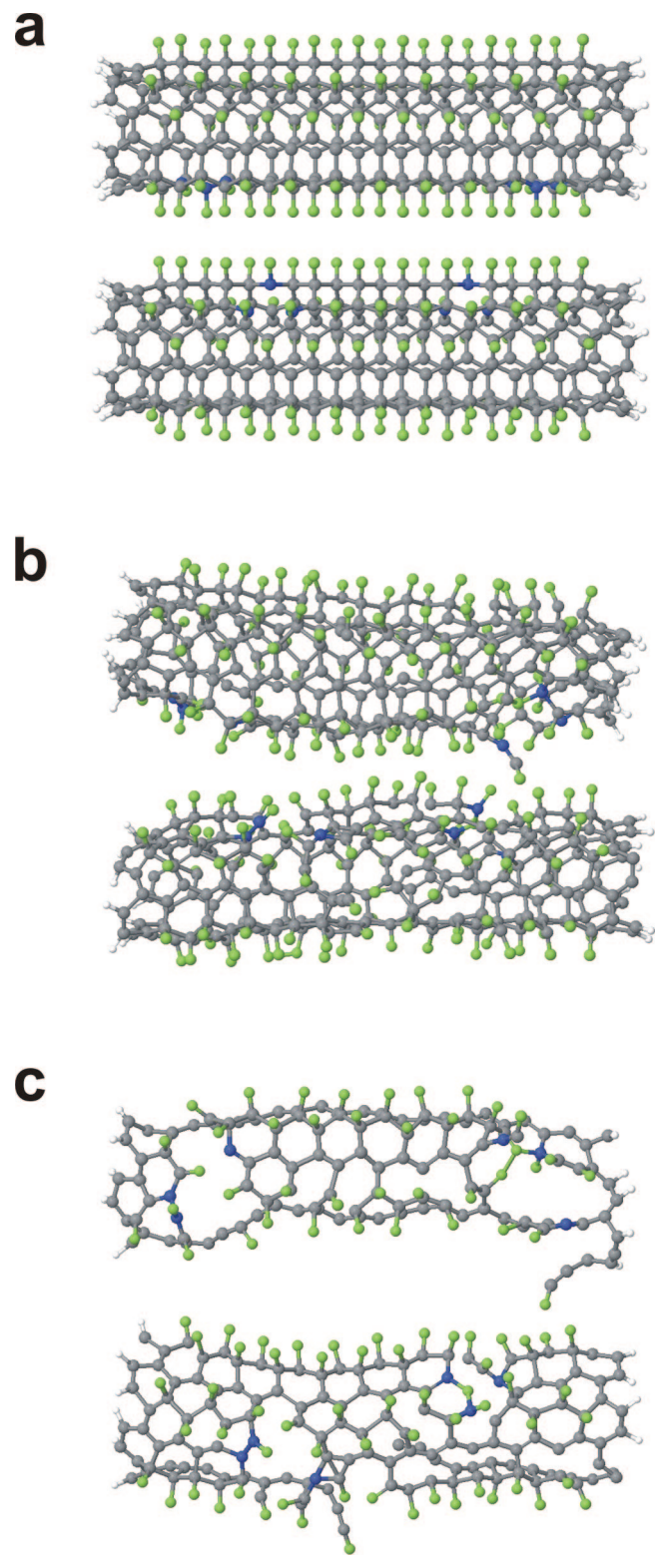

Figure 7. Snapshots of the de-fluorination of fluorinated MWNTs by theoretical molecular dynamics simulations. (a) Starting system for the MD simulations for two adjacent (5,5) $C_{238}F_{100}H_{20}$ carbon nanotubes, each containing two vacancies at their interface. (b) End system of the MD simulations after 450 fs. (c) Side view of the interface for both nanotubes, as observed from the other nanotube's perspective for the end system after 450 fs. The three carbon atoms around each vacancy are indicated in blue throughout.

ing the thermal de-fluorination process, and this could further facilitate the tube surface reconstruction and induce cross-linking between adjacent nanotubes (Figure 7).

On the basis of the results described above, we propose the following mechanism for solidification of carbon nanotubes by de-fluorination. (1) After purification of the MWNTs, some defects (vacancies, carboxyl groups, *etc.*) remain or are created on the surface of the MWNTs. (2) During the fluorination process, F atoms bond covalently mainly to the external surfaces of the tubes, and some reconstruction of the defects could occur by the incorporation of F, C, and O atoms. (3) By pressing and annealing the F-MWNTs, F atoms located close to defective sites react easily with C atoms, thus forming CF_x species that are liberated in the gaseous form. (4) When the CF_x groups leave the surface of the tubes, vacancies are created, and due to their high reactivity, they start interconnecting with other vacancies on the adjacent walls of other nanotubes. (5) Various types of covalent interconnections are created among the nanotubes, and a robust 3D random nanotube network is formed. Interestingly, the resulting materials are lighter than graphite and are robust enough to be machined and polished.

CONCLUSION

Fluorination and de-fluorination of MWNTs appears to be an excellent way to functionalize and interconnect covalently carbon nanotubes. Using this method, it is also possible to obtain blocks that could be processed and polished without using a binder or a polymer matrix. To the best of our knowledge, this method and the obtained materials have not been reported hitherto. We believe this process could be exploited further since the fluorination process is reversible and can be controlled from low degrees of fluorination up to full coverage of the nanotube surface exhibiting C_2F stoichiometries. We have demonstrated that de-fluorination of F-MWNTs results in the creation of vacancies between adjacent tubes that are highly reactive and start interlinking so as to generate covalent networks of MWNTs and robust blocks. It is noteworthy that the produced blocks exhibit mechanical and conducting properties that surpass those found in commercial graphite and other types of nanotube composites. The use of orientated carbon nanotube fibers,[45–48] yarns,[49,50] sheets,[51] films,[52] or forests,[53–55] could even further improve the reported properties and could result in even stronger and highly conducting carbon nanotube-based blocks.

MATERIALS AND METHODS

Purification of MWNTs. The purity of the MWNTs was about 80 wt %, and the rest of the material consisted of amorphous carbon (8.50 wt %), Al (5.73 wt %), Fe (4.43 wt %), Mo (1.27 wt %), and Cr (0.07 wt %); the nanotubes exhibited bamboo-like morphologies. The average tube diameter ranged from 20 to 40 nm, and the lengths ranged from 500 nm to 5.0 μm. The MWNT soot was burned in air at 773 K for 90 min, and the remaining soot was then introduced into a flask containing 6 M HCl in order to dissolve the Fe, Mo, and Cr. Following this procedure, the acid solution was filtered using a membrane filter, and 1.0 g of the filtered material was transferred into a flask with 1.0 L of 2 M NaOH and refluxed at 373 K for 6 h in order to dissolve aluminum oxides. The resulting suspension was then filtered and washed with hot water. Finally, samples were dried *in vacuo* at 373 K for 24 h. After purification, the impurities consisted of Na (0.40 wt %), Al (1.41 wt %), Fe (0.26 wt %), Mo (1.27 wt %), and Cr (0.15 wt %); the elemental analysis was obtained by inductively coupled plasma optical emission spectroscopy (ICP-OES).

Fluorination of MWNTs. The purified MWNTs were fluorinated at 523 K using a mixture of F_2 (20%) and N_2 (80%) for 2 h (flow rate of 25 mL/min). Subsequently, thermal annealing was carried out at 523 K for 6 h in a polytetrafluoroethylene cell under a nitrogen flow of 20 mL/min. The products were then characterized by XPS using an AXIS-His instrument (Kratos Analytical Ltd., UK), and the C:F stoichiometries were determined.

Preparation of COOH-MWNTs. In the same way as mentioned above, the MWNT powder was burned in air at 773 K for 90 min in order to remove unwanted carbonaceous material. At this point, 1.0 g of the burned soot was then introduced into a flask containing 6 M HCl to dissolve the Fe, Mo, and Cr. Following this, the acid solution was filtered, and 500 mg of the washed soot was transferred into a flask with 0.5 L of 6.8 M HNO_3 and refluxed at 373 K for 16 h. The resulting suspension was filtered and washed with distilled water. Finally, the samples were dried *in vacuo* at 373 K for 24 h. After this treatment, impurities (estimated by ICP-OES) in this sample were Al (0.16 wt %), Fe (0.32 wt %), and Mo (0.02 wt %) by ICP-OES.

Production of MWNT Blocks. The de-fluorinated or decarboxylated MWNT blocks were prepared using a SPS system (Sumitomo Coal Mining, SPS-1050, Japan) shown in Figure S1 (Supporting Information). SPS is a unique synthesis and processing technique which makes possible sintering at low temperatures and for short periods of time by charging particles with electrical energy and effectively applying the high energy of a spark plasma. The SPS process experiences a very high thermal efficiency because of the direct heating caused by the spark, and it can easily produce a homogeneous, high-quality sintered product due to the uniform heating generated. Typically, 300 mg of the MWNT powder was used and hardened in a graphite-covered die with a diameter of 20 mm at 1273 K (heating rate, 25 K/min) under a pressure of 80 MPa *in vacuo* (1×10^{-2} Torr) for 10 min. The typical weight loss of de-F-MWNT blocks was 50.0−55.3 wt % of the initial fluorinated MWNT powder. On the other hand, the weight loss of de-COOH-MWNT blocks corresponded to 12.2 wt % of the initial COOH-MWNT powder.

Structural Characterization. The sample morphologies were determined by SEM (S-4100, Hitachi, Japan) and HRTEM (HF-2000, Hitachi, Japan); the instruments were equipped with a field emission gun. The scanning and transmission electron microscopes were operated at 5 and 200 kV, respectively. The transmission electron microscopy had attached a NORAN Instruments energy-dispersive X-ray detector and a Gatan imaging filter with an energy resolution of 1.0 eV. Metal impurities were detected by ICP-OES (Thermo Elemental Co. Ltd., USA). The vibrational modes of the modified nanotube samples were characterized using Fourier transform infrared absorption (Avatar 380, Thermo Electron Co. Ltd., USA). In particular, the samples were measured inside a KBr pellet. Raman scattering spectroscopy (Jobin-Yvon T64000, Horiba Co. Ltd., Japan) studies were used to analyze the vibrational modes of graphitic materials. These measurements were carried out at room temperature using an Ar ion laser (488.0 nm). XPS (used to confirm the fluorination of MWNTs) was performed on an AXIS-His instrument (Kratos Analytical Ltd., UK) with a monochromatized Al Kα line. Thermogravimetry with differential thermal analysis (TG-DTA) (STA 409 PC Luxx, NETZSCH-

Geratebau GmbH, Germany) and mass spectroscopy (QMS 403 C Aëolos, NETZSCH-Geratebau GmbH, Germany) were used to detect the gas products of thermal decomposition of the fluorinated MWNTs in helium (flow rate, 55 cm^3/min) at room temperature and up to 1273 K (10 K/min).

Mechanical Properties. The mechanical properties of the solid blocks—the Young's modulus and fracture strength—were measured using three-point bending tests, which were performed on a universal testing machine (Instron 5582) at atmospheric conditions and room temperature. The load was applied at a crosshead speed of 0.05 mm/min. The Young's modulus E_b and fracture strength σ_b are given by the following equations,

$$E_b = 1/4(L^3/bh^3)P/\delta, \quad \sigma_b = (3P_bL/2bh^2)$$

where L is the span length (16 mm), b the specimen width (2.0 mm), h the specimen thickness (1 mm), P/δ the initial linear slope of the load *versus* load-line displacement curve, and P_b the maximum load. Three specimens were tested, and the averaged results were obtained. The shape of tested specimens was approximately 2.0 × 18 × 1.0 mm. The solid specimens were polished with Emery paper (no. 1200) and Fuji film lapping tape (no. 2000 and no. 4000, Fuji Photo Film Co., Ltd., Japan). Eight tests were made on each material.

Indentation tests were carried out on a HMV-1/2 hardness tester with a diamond Vickers indenter (Shimazu Co. Ltd., Japan). The indentation parameters were a 1.961 N load with a dwell of 15 s. Vickers indentation sites were observed by SEM. Ten tests were performed on each material.

Electrical Conductivity Measurements. The specimens were measured at room temperature on rectangular blocks (2.0 × 18 × 1.0 mm) parallel to their length, *i.e.*, perpendicular to the pressing axis. The solid specimens were polished with Emery paper (no. 1200) and Fuji film lapping tape (no. 2000 and no. 4000, Fuji Photo Film Co., Ltd., Japan). A four-terminal electrical transport method was also carried out using a Solartron 1287 (an electrochemical interface), in combination with a Solartron 1260 (impedance/gain phase analyzer). In this case, the samples had small current electrodes and voltage electrodes in the form of two narrow strips of platinum on the large surface of the block. The frequency range was 1.0 Hz to 3.0 kHz, and the amplitude of the alternate current signal was 10 mV. A two-terminal method was carried out using the above setup. The electrical conductivity of the specimens was measured at room temperature along the rectangular surfaces of the specimens and along the perpendicular direction (thickness).

The electrical conductivity of the nanotube powder was measured using a powder measurement system (Loresta GP MCP-T600, Dia Instruments Co., Ltd., Japan). This experiment was performed at room temperature in the pressure range of 100–650 kgf/cm^2. About 1.0 g of sample was mounted into an electrical insulated mold. First, resistance was measured by holding a metallic electrode against the sample surface (four-probe method recorded at room temperature, in which a pin electrode was deposited every 3.0 mm). Volume resistivity was calculated by multiplying resistance by the resistivity correction factor, determined according to the sample's shape and size. Note that conductivity is the inverse of volume resistivity.

Bulk Density Measurements and Porosity Estimation. All specimens were shaped into rectangular pieces (2.0 × 20 × 1.0 mm). The specimens were polished as described above. Bulk densities of the solids were measured using an analytical electrobalance (GR-202, A & D Co. Ltd., Japan) and a high-precision microscale (M200, Mitutoyo Co., Japan) for length, width, and thickness determinations. The porosity of the solids is given by

$$P = 1 - (d_{bulk}/d_{true})$$

where d_{bulk} is the bulk density of solid and d_{true} the true density of graphite (2.26 g/cm^3).

Acknowledgment. Y.S. thanks Dr. S. Tachizono for assistance. This work was supported by a Grant-in-Aid for Young Research (A) 19686038 and Exploratory Research 19656175 from the Ministry of Education, Science, Culture and Sport of Japan, and Health and Labor Sciences Research Grant No. H18-chemistry-006 from the Ministry of Health, Labor and Welfare (Y.S.). G.V.L. acknowledges the Research Foundation−Flanders (FWO) for financial support as a Postdoctoral Research Fellow and thanks Dr. C. P. Ewels, Prof. J.-C. Charlier, and Prof. P. Geerlings for useful discussions. We also thank CONACYT-México for financial support grants: 56787 (Laboratory for Nanoscience and Nanotechnology Research-LINAN), 45762 (M.T.), 41464-Inter American Collaboration (M.T.), 2004-01-013/SALUD-CONACYT (M.T.), PUE-2004-CO2-9 Fondo Mixto, and the Laboratory for Nanoscience and Nanotechnology Research (LINAN) through grant no. 56787 (M.T.).

Note added after ASAP publication: After this paper was published ASAP February 8, 2008, a production error was corrected in the dimensions of the tested specimens in the Mechanical Properties section. The corrected version was published February 26, 2008.

Supporting Information Available: Preparation and characterization of samples. This material is available free of charge *via* the Internet at http://pubs.acs.org.

REFERENCES AND NOTES

1. Frackowiak, E.; Metenier, K.; Bertagna, V.; Beguin, F. Supercapacitor Electrodes from Multiwalled Carbon Nanotubes. *Appl. Phys. Lett.* **2000**, *77*, 2421–2423.
2. Balasubramanian, K.; Burghard, M. Biosensors Based on Carbon Nanotubes. *Anal. Bioanal. Chem.* **2006**, *385*, 452–468.
3. Aoki, N.; Yokoyama, A.; Nodasaka, Y.; Akasaka, T.; Uo, M.; Sato, Y.; Tohji, K.; Watari, F. Cell Culture on a Carbon Nanotube Scaffold. *J. Biomed. Nanotechnol.* **2005**, *1*, 402–405.
4. Bokros, J. C. Carbon Biomedical Devices. *Carbon* **1977**, *15*, 355–371.
5. Baughman, R. H.; Zakhidov, A. A.; de Heer, W. A. Carbon Nanotubes—The Route toward Applications. *Science* **2002**, *297*, 787–792.
6. Romo-Herrera, J. M.; Terrones, M.; Terrones, H.; Dag, S.; Meunier, V. Covalent 2D and 3D Networks from 1D Nanostructures: Designing New Materials. *Nano Lett.* **2007**, *7*, 570–576.
7. Niyogi, S.; Hamon, M. A.; Hu, H.; Zhao, B.; Bhowmik, P.; Sen, R.; Itkis, M. E.; Haddon, R. C. Chemistry of Single-Walled Carbon Nanotubes. *Acc. Chem. Res.* **2002**, *35*, 1105–1113.
8. Hirsch, A. Functionalization of Single-Walled Carbon Nanotubes. *Angew. Chem., Int. Ed.* **2002**, *41*, 1853–1859.
9. Balasubramanian, K.; Burghard, M. Chemically Functionalized Carbon Nanotubes. *Small* **2005**, *1*, 180–192.
10. Burghard, M. Electronic and Vibrational Properties of Chemically Modified Single-Wall Carbon Nanotubes. *Surf. Sci. Rep.* **2005**, *58*, 1–109.
11. Tasis, D.; Tagmatarchis, N.; Bianco, A.; Prato, M. Chemistry of Carbon Nanotubes. *Chem. Rev.* **2006**, *106*, 1105–1136.
12. Haddon, R. C. Electronic Structure, Conductivity and Superconductivity of Alkali Metal Doped C_{60}. *Acc. Chem. Res.* **1992**, *25*, 127–133.
13. Lucas, A. A.; Lambin, P. H.; Smalley, R. E. On the Energetics of Tubular Fullerenes. *J. Phys. Chem. Solids* **1993**, *54*, 587–593.
14. Ajayan, P. M.; Tour, J. M. Nanotube Composites. *Nature* **2007**, *447*, 1066–1068.
15. Calvert, P. Nanotube Composites: A Recipe for Strength. *Nature* **1999**, *399*, 210–211.
16. Terrones, M.; Terrones, H.; Banhart, F.; Charlier, J. C.; Ajayan, P. M. Coalescence of Single-Walled Carbon Nanotubes. *Science* **2000**, *288*, 1226–1229.
17. Endo, M.; Hayashi, T.; Muramatsu, H.; Kim, Y. A.; Terrones, H.; Terrones, M.; Dresselhaus, M. S. Coalescence of Double-Walled Carbon Nanotubes: Formation of Novel Carbon Bicables. *Nano Lett.* **2004**, *4*, 1451–1454.
18. Khabashesku, V, N.; Gu, Z.; Brinson, B.; Zimmerman, J. L.; Margrave, J. L.; Davydov, V. A.; Kashevarova, L. S.;

Rakhmanina, A. V. Polymerization of Single-Wall Carbon Nanotubes under High Pressures and High Temperatures. *J. Phys. Chem. B* **2002**, *106*, 11155–11162.
19. Kis, A.; Csányi, G.; Salvetat, J. P.; Lee, T. N.; Couteau, E.; Kulik, A. J.; Benoit, W.; Brugger, J.; Forró, L. Reinforcement of Single-Walled Carbon Nanotube Bundles by Intertube Bridging. *Nat. Mater.* **2004**, *3*, 153–157.
20. Mickelson, E. T.; Huffman, C. B.; Rinzler, A. G.; Smalley, R. E.; Hauge, R. H.; Margrave, J. L. Fluorination of Single-Wall Carbon Nanotubes. *Chem. Phys. Lett.* **1998**, *296*, 188–194.
21. Khabashesku, V. N.; Billups, W. E.; Margrave, J. L. Fluorination of Single-Wall Carbon Nanotubes and Subsequent Derivatization Reactions. *Acc. Chem. Res.* **2002**, *35*, 1087–1095.
22. Gu, Z.; Peng, H.; Hauge, R. H.; Smalley, R. E.; Margrave, J. L. Cutting Single-Wall Carbon Nanotubes through Fluorination. *Nano Lett.* **2002**, *2*, 1009–1013.
23. Yusa, H. Nanocrystalline Diamond Directly Transformed from Carbon Nanotubes under High Pressure. *Diamond Relat. Mater.* **2002**, *11*, 87–91.
24. Liu, J. L.; Bai, G. Z.; Feng, J. W.; Jiang, W. Microstructure and Mechanical Properties of Hot-Pressed Carbon Nanotubes Compacted by Spark Plasma Sintering. *Carbon* **2005**, *43*, 2649–2653.
25. Yamamoto, G.; Omori, M.; Sato, Y.; Takahashi, T.; Tohji, K.; Hashida, T. Effects of Polycarbosilane Addition on the Mechanical Properties of Single-Walled Carbon Nanotube Solids. *JSME Int. J. Ser. A—Solid Mech. Mater. Eng.* **2005**, *48*, 189–193.
26. Hamwi, A.; Alvergnat, H.; Bonnamy, S.; Béguin, F. Fluorination of Carbon Nanotubes. *Carbon* **1997**, *35*, 723–728.
27. Yudanov, N. F.; Okotrub, A. V.; Shubin, Y. V.; Yudanova, L. I.; Bulusheva, L. G. Fluorination of Arc-Produced Carbon Material Containing Multiwall Nanotubes. *Chem. Mater.* **2002**, *14*, 1472–1476.
28. Bettinger, H. F.; Peng, H. Thermolysis of Fluorinated Single-Walled Carbon Nanotubes: Identification of Gaseous Decomposition Products by Matrix Isolation Infrared Spectroscopy. *J. Phys. Chem. B* **2005**, *109*, 23218–23224.
29. Tohara, H.; Okino, F. Property Control of Carbon Materials by Fluorination. *Carbon* **2000**, *38*, 241–267.
30. Kawasaki, S.; Komatsu, K.; Okino, F.; Tohara, H.; Kataura, H. Fluorination of Open- and Closed-End Single-Walled Carbon Nanotubes. *Phys. Chem. Chem. Phys.* **2004**, *6*, 1769–1772.
31. Prest, W. M.; Mosher, R. A. In *Colloids and Surfaces in Reprographic Technology*; Hair, M., Croucher, M., Eds.; American Chemical Society: Washington, DC, 1982; pp 255.
32. Shaffer, M. S. P.; Fan, X.; Windle, A. H. Dispersion and Packing of Carbon Nanotubes. *Carbon* **1998**, *36*, 1603–1612.
33. Ogino, S.; Sato, Y.; Yamamoto, G.; Sasamori, K.; Kimura, H.; Hashida, T.; Motomiya, K.; Jeyadevan, B.; Tohji, K. Relation of the Number of Cross-Links and Mechanical Properties of Multi-Walled Carbon Nanotube Films Formed by a Dehydration Condensation Reaction. *J. Phys. Chem. B* **2006**, *110*, 23159–23163.
34. Sato, Y.; Ogawa, T.; Motomiya, K.; Shinoda, K.; Jeyadevan, B.; Tohji, K.; Kasuya, A.; Nishina, Y. Purification of MWNTs Combining Wet Grinding, Hydrothermal Treatment, and Oxidation. *J. Phys. Chem. B* **2001**, *105*, 3387–3392.
35. Yu, M. F.; Lourie, O.; Dyer, M. J.; Moloni, K.; Kelly, T. F.; Ruoff, R. S. Strength and Breaking Mechanism of Multiwalled Carbon Nanotubes under Tensile Load. *Science* **2000**, *287*, 637–640.
36. Cumings, J.; Zettl, A. Low-Friction Nanoscale Linear Bearing Realized from Multiwall Carbon Nanotubes. *Science* **2000**, *289*, 602–604.
37. Wang, X.; Padture, N. P.; Tanaka, H. Contact-Damage-Resistant Ceramic/Single-Wall Carbon Nanotubes and Ceramic/Graphite Composites. *Nat. Mater.* **2004**, *3*, 539–544.
38. Pehrsson, P. E.; Zhao, W.; Baldwin, J. W.; Song, C.; Liu, J.; Kooi, S.; Zheng, B. Thermal Fluorination and Annealing of Single-Wall Carbon Nanotubes. *J. Phys. Chem. B* **2003**, *107*, 5690–5695.
39. Schlegel, H. B.; Millam, J. M.; Iyengar, S. S.; Voth, G. A.; Daniels, A. D.; Scuseria, G. E.; Frisch, M. J. *Ab Initio* Molecular Dynamics: Propagating the Density Matrix with Gaussian Orbitals. *J. Chem. Phys.* **2001**, *114*, 9758–9763.
40. Iyengar, S. S.; Schlegel, H. B.; Millam, J. M.; Voth, G. A.; Scuseria, G. E.; Frisch, M. J. *Ab Initio* Molecular Dynamics: Propagating the Density Matrix with Gaussian Orbitals. II. Generalizations Based on Mass-Weighting, Idempotency, Energy Conservation and Choice of Initial Conditions. *J. Chem. Phys.* **2001**, *115*, 10291–10302.
41. Schlegel, H. B.; Iyengar, S. S.; Li, X.; Millam, J. M.; Voth, G. A.; Scuseria, G. E.; Frisch, M. J. *Ab Initio* Molecular Dynamics: Propagating the Density Matrix with Gaussian Orbitals. III. Comparison with Born—Oppenheimer Dynamics. *J. Chem. Phys.* **2002**, *117*, 8694–8704.
42. Dewar, M. J. S.; Zoebisch, E. G.; Healy, E. F.; Stewart, J. J. P. Development and Use of Quantum Mechanical Molecular Models. 76. AM1: A New General Purpose Quantum Mechanical Molecular Model. *J. Am. Chem. Soc.* **1985**, *107*, 3902–3909.
43. Frisch, M. J.; Trucks, G. W.; Schlegel, H. B.; Scuseria, G. E.; Robb, M. A.; Cheeseman, J. R.; Montgomery, J. A., Jr.; Vreven, T.; Kudin, K. N.; Burant, J. C., *et al. Gaussian 03*, Revision B.05; Gaussian, Inc.: Pittsburgh, PA, 2003.
44. Van Lier, G.; Ewels, C. P.; Zuliani, F.; De Vita, A.; Charlier, J. C. Theoretical Analysis of Fluorine Addition to Single-Walled Carbon Nanotubes: Functionalization Routes and Addition Patterns. *J. Phys. Chem. B* **2005**, *109*, 6153–6158.
45. Vigolo, B.; Pénicaud, A.; Coulon, C.; Sauder, C.; Pailler, R.; Journet, C.; Bernier, P.; Poulin, P. Macroscopic Fibers and Ribbons of Oriented Carbon Nanotubes. *Science* **2000**, *290*, 1331–1334.
46. Zhu, H. W.; Xu, C. L.; Wu, D. H.; Wei, B. Q.; Vajtai, R.; Ajayan, P. M. Direct Synthesis of Long Single-Walled Carbon Nanotube Strands. *Science* **2002**, *296*, 884–886.
47. Li, Y. L.; Kinloch, I. A.; Windle, A. H. Direct Spinning of Carbon Nanotube Fibers from Chemical Vapor Deposition Synthesis. *Science* **2004**, *304*, 276–278.
48. Ericson, L. M.; Fan, H.; Peng, H.; Davis, V. A.; Zhou, W.; Sulpizio, J.; Wang, Y.; Booker, R.; Vavro, J.; Guthy, C. Macroscopic, Neat, Single-Walled Carbon Nanotube Fibers. *Science* **2004**, *305*, 1447–1450.
49. Jiang, K.; Li, Q.; Fan, S. Spinning Continuous Carbon Nanotube Yarns. *Nature* **2002**, *419*, 801–801.
50. Zhang, M.; Atkinson, K. R.; Baughman, R. H. Multifunctional Carbon Nanotube Yarns by Downsizing an Ancient Technology. *Science* **2004**, *306*, 1358–1361.
51. Zhang, M.; Fang, S.; Zakhidov, A. A.; Lee, S. B.; Aliev, A. E.; Williams, C. D.; Atkinson, K. R.; Baughman, R. H. Strong, Transparent, Multifunctional, Carbon Nanotube Sheets. *Science* **2005**, *309*, 1215–1219.
52. Du, C.; Yeh, J.; Pan, N. Carbon Nanotube Thin Films with Ordered Structures. *J. Mater. Chem.* **2005**, *15*, 548–550.
53. Ren, Z. F.; Huang, Z. P.; Xu, J. W.; Wang, J. H.; Bush, P.; Siegal, M. P.; Provencio, P. N. Synthesis of Large Arrays of Well-Aligned Carbon Nanotubes on Glass. *Science* **1998**, *282*, 1105–1107.
54. Cao, A.; Dickrell, P. L.; Sawyer, W. G.; Ghasemi-Nejhad, M. N.; Ajayan, P. M. Super-Compressible Foamlike Carbon Nanotube Films. *Science* **2005**, *310*, 1307–1310.
55. Futaba, D. N.; Hata, K.; Yamada, T.; Hiraoka, T.; Hayamizu, Y.; Kakudate, Y.; Tanaike, O.; Hatori, H.; Yumura, M.; Iijima, S. Shape-Engineerable and Highly Densely Packed Single-Walled Carbon Nanotubes and Their Application as Super-Capacitor Electrodes. *Nat. Mater.* **2006**, *5*, 987–994.